International Journal of Engineering and Technology Innovation, vol. 16, no. 1, 2026, pp. 81-94

Power Generation Optimization of Reverse Electrodialysis: Effects of Key Operating and Design Parameters

Po-Hsun Lin[1,*], Cheng-Huan Tsai[1], Ching-Lung Chen[2], Chi-Chen Lin[1]

[1]Graduate Institute of Environmental Engineering, National Central University, Taoyuan, Taiwan, ROC

[2]Department of Safety, Health and Environmental Engineering; Center for Environmental Sustainability and Human Health, Ming Chi University of Technology, New Taipei City, Taiwan, ROC

Received 12 September 2025; received in revised form 21 January 2026; accepted 22 January 2026

DOI: https://doi.org/10.46604/ijeti.2026.15684

Abstract

Salinity gradient power (SGP) via reverse electrodialysis (RED) is a promising renewable energy source; however, maximizing efficiency requires balancing complex electrochemical and hydraulic variables. This study systematically investigates the effects of key operating and design parameters on RED power generation to improve energy efficiency. Laboratory-scale RED experiments are conducted by varying the concentrations of high-concentration (HC) and low-concentration (LC) NaCl solutions, space velocity, the number of ion-exchange membrane (IEM) pairs, and flow channel thickness. The results show that power density increases with concentration ratio and absolute solution concentration, with optimal performance achieved at HC concentrations of 1-2.5 M, LC concentrations of 0.02-0.05 M, and a concentration ratio above 50:1. An optimal space velocity of 0.25 1/min is identified. Increasing the number of IEM pairs enhances power density, while flow channel thicknesses of 1-2 mm minimize resistance. Under optimized conditions, a maximum power density of 0.446 W per square meter is achieved.

Keywords: power generation, renewable energy, reverse electrodialysis, salinity gradient power, space velocity

1. Introduction

The accelerating pace of industrialization worldwide has significantly increased global energy demand, rendering energy sustainability a critical and urgent issue. Concurrently, atmospheric carbon dioxide (CO_2) concentrations have exceeded 400 parts per million (ppm), emphasizing the necessity of transitioning from fossil fuels to renewable energy sources. Conventional renewable energy technologies, such as solar, wind, hydro, geothermal, and blue energy, have gained increasing attention due to their potential to reduce carbon emissions. Among these, salinity gradient power (SGP) shows the lowest carbon emissions. This characteristic makes it one of the most environmentally benign power generation technologies available. It is estimated that global-scale mixing of seawater and freshwater could generate approximately 2 terawatts (TW) of electricity through SGP [1].

The power generation performance of reverse electrodialysis (RED) is governed by three primary factors: the feed solution properties, the ion-exchange membranes (IEMs), and the electrode system. Among these, the characteristics of the feed solution critically influence the salinity gradient, which in turn determines the energy conversion efficiency of the RED process. The ionic composition of the feed solution is particularly important, as different ions vary in hydration radius and transport behavior.

* Corresponding author. E-mail address: phlin@ncu.edu.tw

Sodium chloride (NaCl) is commonly used in RED systems due to its favorable ion transport characteristics. In contrast, multivalent ions are known to induce the uphill transport effect, which impedes net ion migration and reduces power generation efficiency [2-3]. Emdadi et al. [4] also demonstrated that increasing the sulfate ion (SO_4^{2-}) concentration in the low-concentration (LC) solution from 0.01 M to 0.1 M reduces the open circuit voltage (OCV) by approximately 41%. This decline is primarily attributed to a decrease in the Nernst potential and the occurrence of uphill transport. To maintain charge neutrality and Donnan equilibrium between the two sides of the IEMs, SO_4^{2-} ions are driven uphill from the diluted channel back to the concentrated channel against their own concentration gradient [4]. Moreover, natural water sources, particularly seawater, contain various impurities such as suspended solids, colloids, and microorganisms, which can lead to fouling of IEMs. Fouling increases membrane resistance and hinders ion selectivity and transport [5-6]. Therefore, appropriate pretreatment of the feed solution is essential to maintain system performance and prolong membrane lifespan.

The second critical factor is solution concentration, which directly determines the membrane potential and, consequently, the power output of the RED system. Ortiz-Martínez et al. [7] used 0.55 M NaCl as a high-concentration (HC) solution and 0.02 M NaCl as an LC solution in a RED stack with 20 IEM cell pairs, which achieves optimal power generation. However, there remains scope for further investigation into the effects of different concentration combinations and ratios of the HC and LC. The third key parameter is the space velocity (i.e., flow rate) of the feed solutions. Space velocity influences both the local concentration gradient and the internal resistance of the system. Variations in HC and LC residence time across the membrane stack affect ion transfer and hydraulic loss, ultimately altering ion transport efficiency and power density. Reducing the residence time enhances power density but simultaneously increases hydraulic losses due to higher pump speeds [8]. Therefore, optimization of flow rate is necessary to achieve maximum performance, and the optimal value may vary depending on the specific configuration and scale of the RED system.

The IEM is a core component in the RED system, functioning as a selective barrier that facilitates unidirectional ion transport between the HC and LC compartments. IEM properties, including material composition, chemical and mechanical stability, swelling degree (SD), ion-exchange capacity (IEC), fixed charge density (FCD), and mechanical rigidity, directly influence membrane selectivity, system resistance, and output voltage [9-14]. Given that IEMs account for a significant proportion of the capital cost in RED systems, cost reduction is essential for large-scale deployment, particularly in seawater desalination applications. Ranade et al. [15] reported that the membrane price should be reduced to 5 €/m² to achieve economic viability compared to the current price of membranes, approximately 50 €/m², which highlights that the development of low-cost, high-performance membranes is crucial for the commercialization of RED technologies.

In addition to the aforementioned factors, other parameters such as membrane properties, electrode design, solution temperature, and module geometry also play important roles in affecting system performance [16-18]. This study investigated the effects of operational parameters on the power generation performance of a RED system. The primary objective is to experimentally evaluate the energy production efficiency of the RED system under varying conditions. This study distinguishes itself by moving beyond binary salt-gradient testing to evaluate the space velocity metric, which provides a more intuitive and scalable comparison across different RED stack dimensions than simple flow rates. Furthermore, this research specifically quantified the exact threshold at which the flow channel thickness shifted from a benefit to a performance-limiting resistance, offering a precise roadmap for industrial-scale stack design that is scarcely addressed in existing literature.

2. Materials and Methods

In a RED system, cation-exchange membranes (CEMs) and anion-exchange membranes (AEMs) are alternately arranged in parallel between two electrodes (Fig. 1(a)). Spacers and gaskets are used to separate the IEMs, forming a series of compartments. An anode is positioned in the electrode chamber next to the freshwater compartment, while a cathode is placed adjacent to the HC solution compartment. An electrode rinse solution circulates between the anode and cathode chambers (Fig.

1(b)). Alternating streams of HC and dilute solutions are introduced into the respective compartments. Due to the salinity gradient between the two solutions, an electric potential (membrane potential) develops across the IEMs. This salinity gradient drives ions from the high-concentration compartments to the low-concentration compartments. The cations ultimately move toward the cathode, and the anions toward the anode. The redox reaction that occurs at the electrodes releases electrons to maintain electroneutrality. These electrons flow through an external circuit from the anode to the cathode, generating an electric current [19-21].

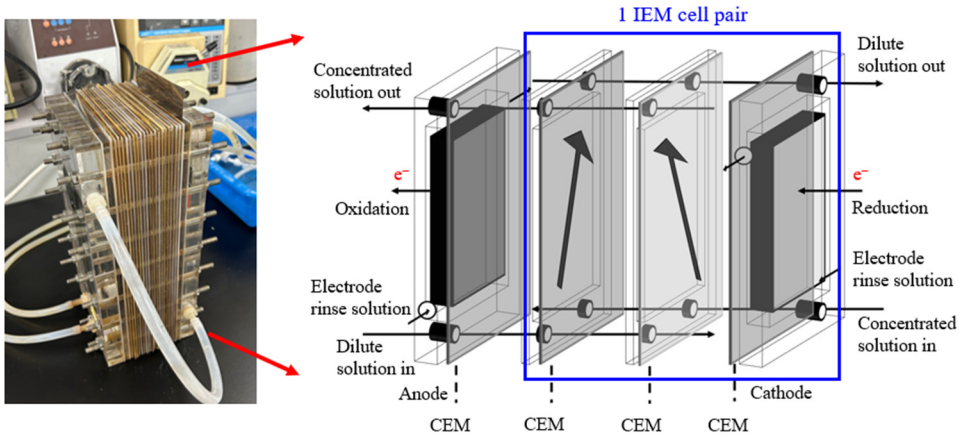

(a) RED structure and solution flow direction

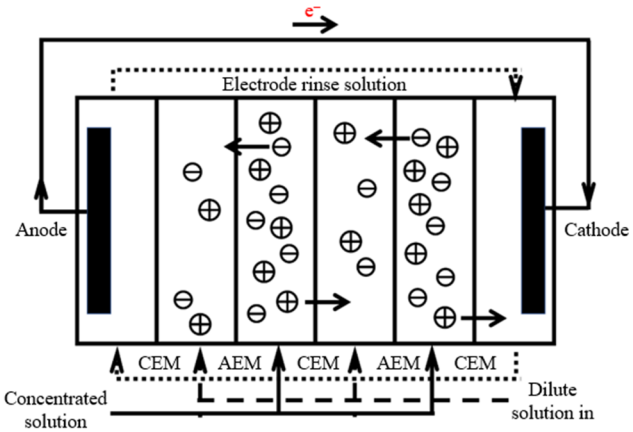

(b) RED power generation mechanism

Fig. 1 Schematic diagram of the RED system [20]

The objective of this research is to investigate the parameters affecting RED power generation and to optimize the operating conditions by adjusting the concentrations and space velocities of HC and LC solutions, the number of IEM pairs, and the flow channel thickness. The RED stack is configured with 1 to 5 cell pairs, depending on the experimental conditions, with an effective area of 67.5 cm² per membrane. The electrode system consists of a mesh-type platinum-coated titanium (Pt/Ti) cathode and a mesh-type dimensionally stable anode (DSA) with an IrO_2/Ta_2O_5 coating. These materials are selected to ensure electrochemical stability and efficient redox reactions during power generation.

The IEMs used include CEMs (CIMS, ASTOM, Japan) and AEMs (ACS, ASTOM, Japan) (Table 1). Acrylic spacers and silicone gaskets, both with a thickness of 1 mm, were used in the RED stack. The HC and LC solutions for RED were prepared with varying concentrations of NaCl, and an electrode rinse solution consisted of a 0.02 M ferricyanide/ferrocyanide redox couple ($K_3[Fe(CN)_6]/K_4[Fe(CN)_6]$), which was continuously circulated through the cathode and anode compartments to facilitate electron transfer and maintain electroneutrality in the RED system. Masterflex peristaltic pumps (Cole-Parmer, USA) were used to pump the HC, LC, and electrolyte solutions. A potentiostat (SP-150, AUBOTECH) was employed to monitor OCV, resistance, voltage, and current, while the conductivity of both the HC and LC solutions at the inlet and outlet was measured to observe concentration variations.

Table 1 The characteristics of IEM used in this experiment

IEM	Resistance (Ω·cm²)	Bursting strength (MPa)	Thickness (mm)	Temperature (℃)	pH
CIMS	4.5	≥ 0.4	0.21	≤ 60	0 to 14
ACS	3.8	≤ 0.15	0.13	≤ 40	0 to 8

In this study, space velocity was used to represent the velocity of the HC and LC solutions flowing into the RED stack. Space velocity is defined as the inverse of residence time. Due to variations in RED system dimensions and the number of IEMs used, conventional expressions (i.e., flow rate) may not provide an intuitive comparison. Instead, space velocity offers a more meaningful metric, as its numerical value is inversely related to the residence time; higher space velocity values indicate shorter residence times and faster flow through the RED stack.

2.1. RED power density calculation

The power output of RED is fundamentally driven by the salinity gradient between the HC and LC solutions. The mixing of these solutions can be interpreted as a change in Gibbs free energy between the two phases. Accordingly, the OCV of the RED cell, denoted as E (V), can be estimated using the Nernst equation [22]:

$$E = \frac{N_m \alpha RT}{zF} \ln\left(\frac{\gamma_{HC} C_{HC}}{\gamma_{LC} C_{LC}}\right) \tag{1}$$

where N_m is the number of IEM cell pairs of the RED system, α is the permeability coefficient of IEM, R is the universal gas constant (8.314 J/(mol·K)), T is the absolute temperature (K), z is the ion valence, F is the Faraday constant (96485 C/mol), γ is the ion activity coefficient, and C is the molar concentration of the feed solution (M). It is important to note that the OCV derived from the theoretical Nernst equation may differ from experimental values due to assumptions of ideal conditions. Therefore, in practical applications, direct measurement of OCV is recommended for a more accurate assessment of RED system performance. Given the OCV, the actual output voltage U of the RED system can be calculated using Ohm's law, as shown below [22]:

$$U = E - JA_m R_{stack} \tag{2}$$

where E is the measured OCV, J is the current density of the RED cell (A/m²), A_m is the effective area of the IEM (m²), and R_{stack} is the internal resistance of the RED stack (Ω). Both E and J can be determined experimentally using a potentiostat. R_{stack} was calculated based on Ohm's law, using the difference between the OCV and the operating voltage under steady-state current conditions. Finally, the power density of the RED system P_d can be determined from the product of U and the total current I, normalized by the number of IEM pairs N_m and the membrane area, as described below [11]:

$$P_d = \frac{UI}{N_m A_m} \tag{3}$$

2.2. Concentration effects of HC and LC solutions

Two sets of experiments were conducted to investigate the effect of HC and LC solution concentrations on the power output of the RED system.

(1) The concentration of the HC solution was fixed at 1 M NaCl, with a space velocity of 0.25 1/min (flow rate: 47.5 mL/min). Four different LC solution concentrations, 0.01, 0.02, 0.05, and 0.1 M NaCl, were tested to evaluate the RED system performance.

(2) The concentration of the LC solution was fixed at 0.02 M NaCl, with the space velocity maintained at 0.25 1/min. Four HC solution concentrations, 2, 1, 0.4, and 0.2 M NaCl, were examined. The current and voltage for each test were recorded to calculate the power output and power density.

2.3. Effects of operating parameters on RED performance

The experiment was conducted using 1 M NaCl and 0.02 M NaCl (concentration ratio of 50:1), with a space velocity of 0.25 1/min for both HC and LC solutions. The following experimental conditions were evaluated to measure the power generation performance of the RED system.

Effects of space velocities

The concentration of the HC solution was fixed at 1 M NaCl, with a space velocity of 0.25 1/min (flow rate: 47.5 mL/min). The LC solution concentration was maintained at 0.02 M NaCl, while its space velocity was varied at 1 1/min (190 mL/min), 0.75 1/min (142.5 mL/min), 0.5 1/min (95 mL/min), 0.375 1/min (71.25 mL/min), and 0.25 1/min (47.5 mL/min). In addition, the LC solution concentration was fixed at 0.02 M NaCl, with a space velocity of 0.25 1/min, while the HC solution concentration was held at 1 M NaCland its space velocity was adjusted to 1 1/min, 0.75 1/min, 0.5 1/min, and 0.25 1/min.

Effects of IEM pairs

Based on the optimal space velocity determined from the above experiments, the effects of the number of IEM pairs on RED power generation were further evaluated. The experimental conditions included an HC solution of 1 M NaCl and an LC solution of 0.02 M NaCl. The number of IEM pairs was systematically varied from 1 to 5 to assess its impact on power generation. Given the high cost of IEMs, it is important to balance the number of IEMs used with the efficiency of RED power generation.

Effects of flow channel thickness

Furthermore, as the flow channel thickness decreases, the solution resistance also decreases. However, in practical applications, fabricating thinner flow channels presents challenges, including structural fragility, potential cracking, and bending, which may compromise the integrity of the system during assembly and operation. Therefore, the effects of flow channel thickness on the resistance of the RED system were investigated using the optimal space velocity. The RED stack was configured with a single pair of IEMs and flow channel thicknesses of 1, 2, 3, and 4 mm. The experiment was conducted using an HC solution of 1 M NaCl and an LC solution of 0.02 M NaCl to assess its effects on system resistance and power generation.

3. Results and Discussions

This section presents and discusses the experimental results obtained from the RED system under various operating conditions. The effects of key parameters, including the concentrations of HC and LC solutions, space velocity, the number of IEM pairs, and flow channel thickness, on OCV, internal resistance, and power density are systematically analyzed. These insights provide a basis for identifying optimal operating windows and for guiding the design of efficient RED systems.

3.1. Concentration effects of HC and LC solutions

Effect of the LC solution concentrations

The concentrations of the HC and LC solutions were set at 1–0.01 M, 1–0.02 M, 1–0.05 M, and 1–0.1 M NaCl (HC–LC), corresponding to concentration ratios of 100:1, 50:1, 20:1, and 10:1, respectively. The OCV, system resistance, and power generation performance of the RED system are presented in Fig. 2. The results indicated that the OCV of the RED system decreased as the concentration of the LC solution increased (Fig. 2(a)), demonstrating that the Gibbs free energy difference between the HC and LC solutions diminished with a decreasing salinity gradient. The relationship between power density and voltage followed a trend similar to that of OCV and resistance, whereby the power density decreased as the LC solution concentration increased (Fig. 2(b)). These results suggest that the power density is predominantly influenced by the concentration ratio at a constant space velocity, with OCV serving as the primary contributing factor.

Specifically, under concentration ratios of 100:1 and 50:1, the OCV difference was relatively small (decreasing by approximately 9.7%), whereas the resistance difference was substantial (decreasing by 73%). In contrast, between concentration ratios of 50:1 and 20:1, the OCV difference was larger (approximately 30.9%), while the resistance difference was relatively minor (14.4%). The power density values obtained in this experiment were 0.346, 0.328, 0.238, and 0.162 W/m² at concentration ratios of 100:1, 50:1, 20:1, and 10:1, respectively. The observed power density trends aligned with the variations in OCV, confirming that OCV played a dominant role in determining RED performance [23].

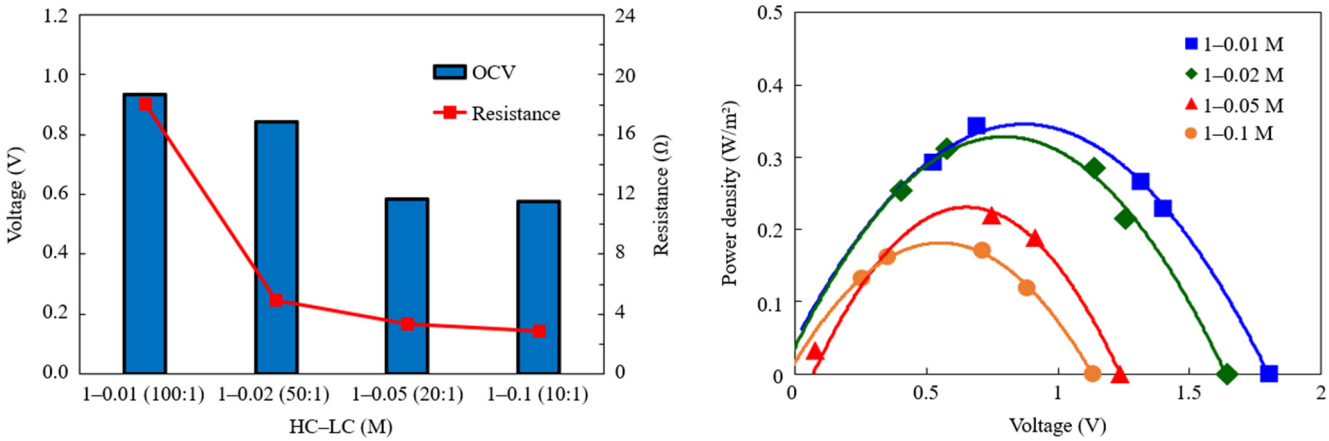

(a) OCV and internal resistance as functions of LC solution concentration

(b) Power density–voltage characteristics at different concentration ratios

Fig. 2 Power generation performance of the RED system at different LC solution concentrations

Effect of the HC solution concentrations

The tested concentration pairs were 2–0.02 M, 1–0.02 M, 0.4–0.02 M, and 0.2–0.02 M NaCl (HC–LC), corresponding to concentration ratios of 100:1, 50:1, 20:1, and 10:1, respectively. The OCV, system resistance, and power generation performance of the RED stack are presented in Fig. 3. The results indicated that the OCV of the RED system increased as the concentration of the HC solution increased (Fig. 3(a)), demonstrating that the free energy difference between the HC and LC solutions was enhanced with an increasing salinity gradient. The power density values obtained in this experiment were 0.446, 0.328, 0.238, and 0.162 W/m² at concentration ratios of 100:1, 50:1, 20:1, and 10:1, respectively (Fig. 3(b)). Furthermore, the power density of the RED system increased with increasing HC solution concentration. These results indicate that increasing the HC solution concentration to elevate the concentration ratio did not significantly influence power density through changes in internal resistance. Among the four tested concentration conditions, the trend in OCV was more consistent with the trend in power density than that of resistance. This observation is consistent with the results discussed above.

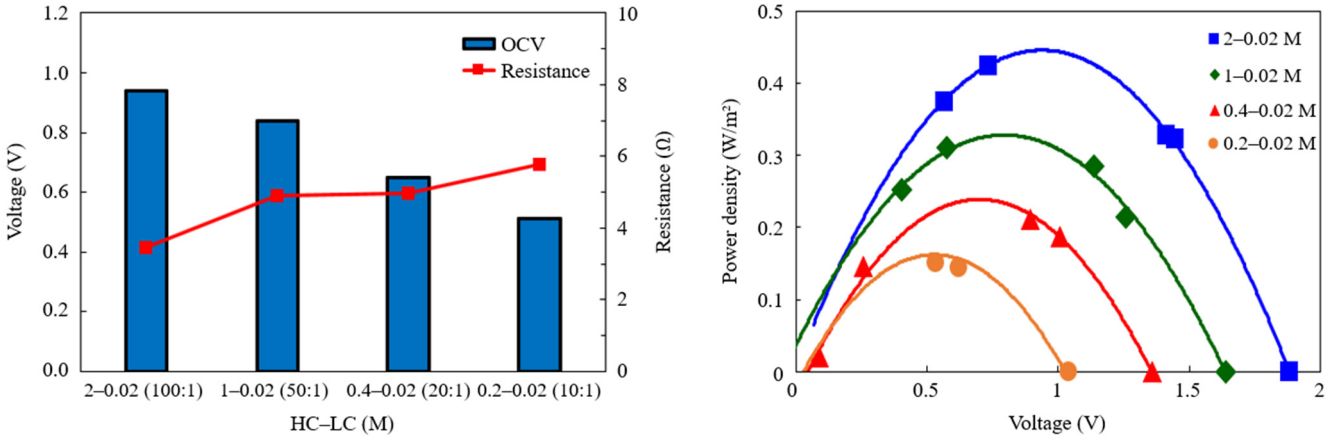

(a) OCV and internal resistance as functions of HC solution concentration

(b) Power density–voltage characteristics at different concentration ratios

Fig. 3 Power generation performance of the RED system at different HC solution concentrations

Fig. 4 presents a summary graph integrating the results from Figs. 2 and 3, illustrating the relationships among power density, internal resistance, and concentration ratio in the RED system. As shown in the figure, increasing the concentration ratio generally leads to a higher power density due to the enhanced Gibbs free energy available from the salinity gradient. However, Fig. 4 also indicates that the concentration ratio alone is insufficient to fully predict power output. When the LC concentration becomes excessively low, the system resistance increases markedly due to reduced ionic conductivity, which offsets the benefit of higher OCV and ultimately limits power density (i.e., 1–0.01 M condition). Based on the results discussed above, the influence of feed solution concentration on RED performance can be categorized into three factors: LC solution concentration, HC solution concentration, and concentration ratio, which are discussed below.

(1) Optimal LC solution concentration (0.02–0.05 M)

To maximize the free energy difference between the HC and LC solutions, the HC solution should be maintained at a higher salinity while the LC solution remains at a lower salinity. A greater free energy difference enhances the OCV in the RED system. However, excessively low LC solution concentrations can lead to a substantial increase in internal resistance, thereby reducing overall system performance. Maintaining the LC solution concentration within the range of 0.02–0.05 M provides an optimal balance between energy potential and electrical resistance, ensuring efficient power generation.

(2) Effect of HC solution concentration

Increasing the HC solution concentration can enhance the free energy difference, which can improve RED performance. However, the practical availability and cost of brine must be considered. Experimental results showed that the highest power density of 0.446 W/m² was achieved under 2–0.02 M conditions. Nonetheless, observations revealed that the internal resistance of the RED stack did not vary significantly when the HC solution concentration ranged from 0.2 to 2 M. In fact, a lower system resistance was recorded under the 1–0.1 M condition (2.91 Ω) compared to the 2–0.02 M condition (3.47 Ω) (Fig. 4). This indicates that RED system resistance is affected more strongly by the concentration of the LC solution than by that of the HC solution.

In addition, the results presented above indicate that an HC solution in the range of 1 to 2 M NaCl produces relatively higher power densities in RED systems. Given that the salinity of natural seawater is approximately 0.6 M NaCl, it is recommended to utilize brine discharge from seawater desalination plants, with salinity levels ranging from approximately 1.2 to 1.4 M NaCl, as the HC solution. This approach can provide a more favorable concentration gradient and enhance the power generation performance of the RED system.

(3) Optimal concentration ratio (≥ 50:1)

The concentration ratio directly influences the free energy difference between the feed solutions and significantly affects OCV. Since power density closely follows the trend of OCV, maintaining a concentration ratio of at least 50:1 is essential for maximizing RED efficiency. The results discussed above confirm that the trends in power density closely follow the trends in OCV, particularly in response to variations in the HC solution. Under the same concentration ratio of 100:1, the RED system exhibited superior performance with a 2–0.02 M condition compared to 1–0.01 M (0.446 W/m² > 0.346 W/m²; 3.47 Ω < 18.07 Ω) (Fig. 4). This is attributed to the significantly higher internal resistance observed in the LC solutions at extremely low concentrations.

A practical implication is that the concentration ratio alone is not sufficient to describe performance, because LC conductivity can dominate the overall ohmic loss. This is also reflected in the literature (Table 2), where, despite a high HC–LC ratio, very dilute LC conditions are consistently associated with low power density due to resistance penalties [24-25]. In contrast, higher power densities reported for larger stack sizes are typically accompanied by sufficiently conductive feed

solutions and/or operating conditions that mitigate polarization [26]. Therefore, the operating window identified here (HC: 1–2 M, LC: 0.02–0.05 M, and ratio ≥ 50:1) should be interpreted as a balance between thermodynamic driving force and resistance control, rather than as a recommendation to maximize the ratio by further diluting the LC solution.

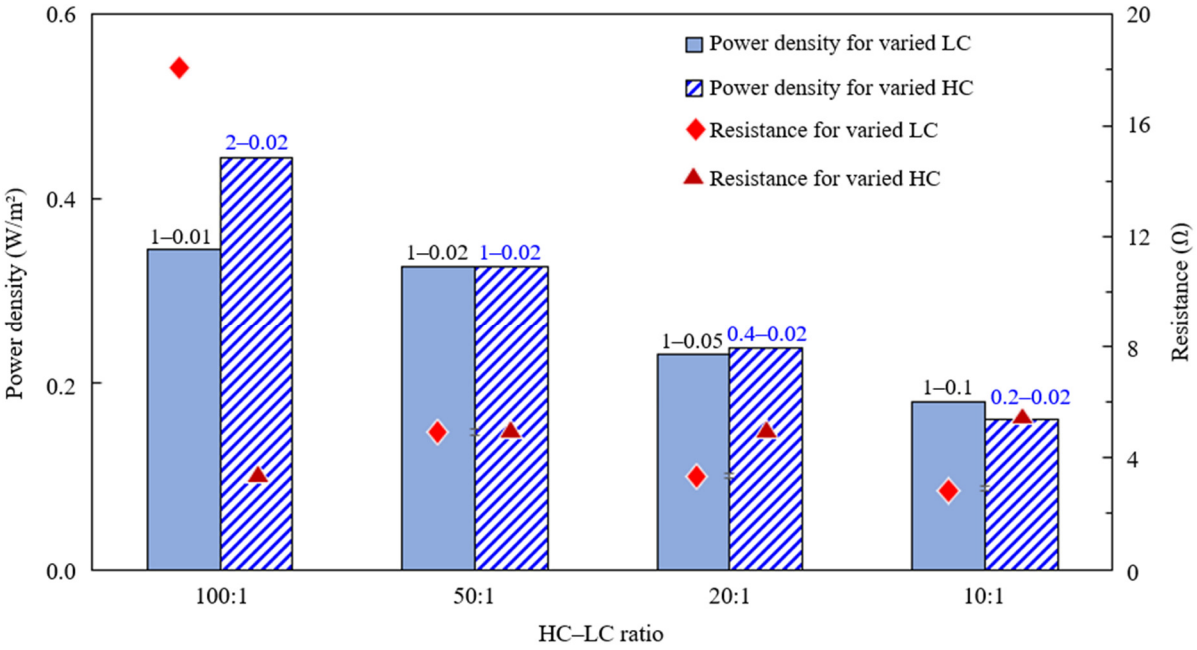

Fig. 4 Summary of power density and internal resistance at different concentration ratios in the RED system

3.2. *Effects of space velocities*

Effect of LC solution space velocity

Fig. 5(a) shows the OCV and system resistance at different LC solution space velocities. When the LC solution space velocity was varied from 0.25 to 1 1/min, the OCV remained relatively stable, ranging between 0.81 and 0.85 V. This indicates that the LC space velocity has no significant effect on the OCV of the RED system. However, variations in space velocity affected the resistance of the IEM by influencing the electric double-layer resistance and the diffusion boundary-layer resistance. A slight increasing trend in total system resistance was observed with increasing space velocity, although the variation was not substantial. The power density as a function of voltage at different space velocities is illustrated in Fig. 5(b). The power density decreased with increasing LC solution space velocity, with the highest value observed at a space velocity of 0.25 1/min (0.375 W/m²).

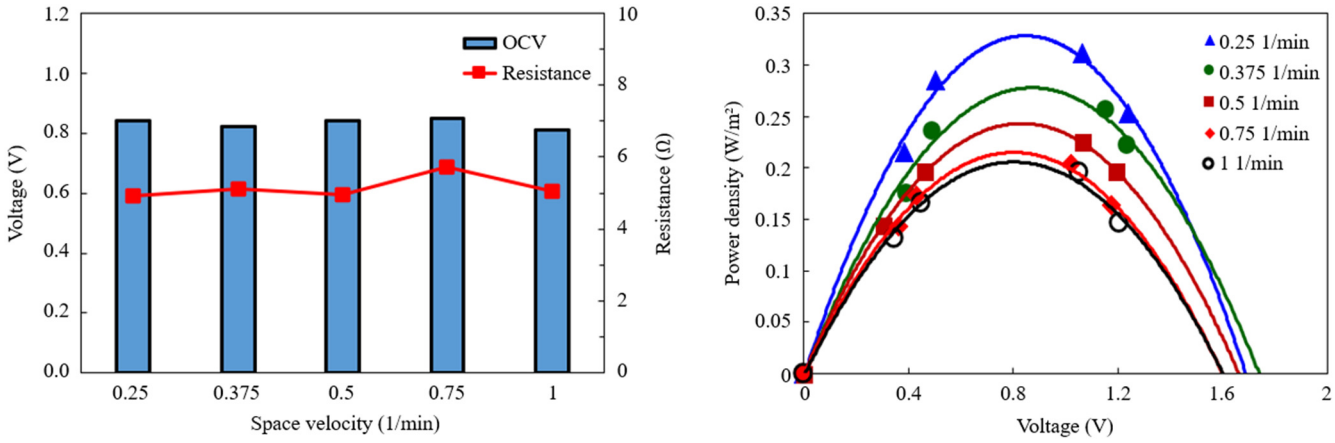

(a) OCV and internal resistance at different LC space velocities

(b) Power density versus voltage at different LC space velocities

Fig. 5 Effect of LC solution space velocity on RED system performance (5 IEM pairs; HC: 1 M, LC: 0.02 M)

As the space velocity increased from 0.25 to 0.375 1/min, the power density dropped from 0.328 to 0.279 W/m² (approximately 15%). At the highest tested space velocity of 1 1/min, the power density further declined to 0.206 W/m². These results suggest that increasing the LC space velocity has an adverse effect on RED power output, despite minimal changes in OCV and internal resistance. While higher space velocity can compress the diffusion boundary layer at the membrane surface, it may also hinder effective ion diffusion and exchange within the solution, thereby reducing the system's power density. Furthermore, increasing the space velocity requires greater energy input for pumping, which ultimately lowers the net energy output of the RED system.

Effect of HC solution space velocity

In this experiment, the space velocity of the LC solution was maintained at 0.25 1/min, while the space velocity of the HC solution was varied at 0.125, 0.25, 0.375, and 0.5 1/min. Fig. 6(a) shows that corresponding OCVs at HC space velocities of 0.125, 0.25, 0.375, and 0.5 1/min, were 0.81, 0.84, 0.82, and 0.87 V, respectively, while the internal resistances were 5.44, 4.91, 5.01, and 4.99 Ω. These results indicate that variations in HC space velocity had no significant effect on OCV. However, space velocity slightly affected the resistance of the IEMs, with a minor decreasing trend observed as space velocity increased. Fig. 6(b) presents the power density as a function of voltage at different HC solution space velocities. Power density initially increased with rising HC space velocity, reaching a peak when the space velocity increased from 0.125 to 0.25 1/min, with power density improving from 0.325 to 0.328 W/m² (increase of approximately 7.5%).

Further increases in space velocity resulted in a decline in power density, dropping to 0.231 W/m² at a space velocity of 0.5 1/min. The results suggest that while excessively low HC solution space velocity limits ion transport and reduces power output, excessively high space velocities are also detrimental to RED performance. Compared to the effect of LC solution space velocity at low values, variations in HC space velocity have a smaller impact on RED power density under low space velocity conditions. Overall, changes in either HC or LC solution space velocity did not lead to significant variations in OCV or internal resistance. However, the data clearly show that increasing HC solution space velocity beyond an optimal point reduces power generation efficiency and requires higher energy input for pumping, thereby diminishing the net energy output of the RED system.

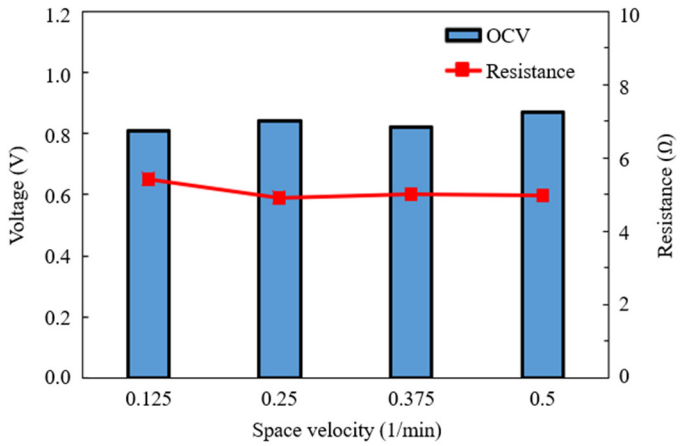

(a) OCV and internal resistance at different HC space velocities

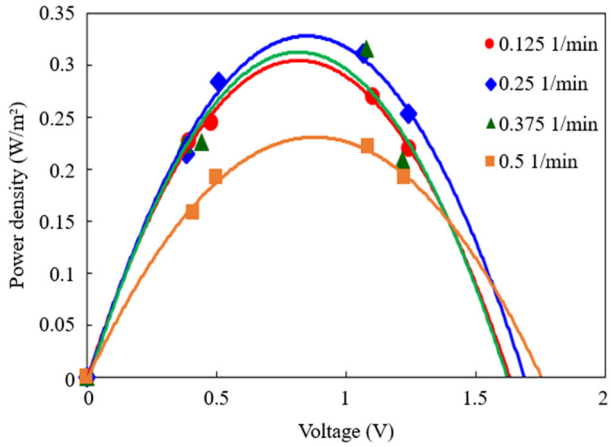

(b) Power density versus voltage at different HC space velocities

Fig. 6 Effect of HC solution space velocity on RED system performance (5 IEM pairs; HC: 1 M, LC: 0.02 M)

Space velocity introduces an electrochemical–hydraulic trade-off. While higher flow can enhance mass transport and mitigate concentration polarization, it can also reduce residence time for effective ion exchange and increase pumping demand, which becomes critical when energy efficiency is considered. This trade-off is evident from prior studies that employed substantially higher space velocities to boost reported power densities [26-27]. Such conditions can improve mass transport but

require greater hydraulic input and may not translate into improved net performance. In this work, the optimum space velocity of approximately 0.25 1/min represents a practical operating point where transport limitations are controlled without imposing excessive hydraulic burden.

3.3. *Effects of IEM pairs*

The relationship between OCV and internal resistance as a function of the number of IEM pairs is presented in Fig. 7(a). The RED stack used an HC solution of 1 M NaCl and an LC solution of 0.02 M NaCl. Both solutions were circulated at a space velocity of 0.25 1/min. When the RED system employed 1 to 5 IEM pairs, the corresponding OCV values were 0.195, 0.345, 0.515, 0.609, and 0.842 V, respectively. The OCV increased proportionally with the number of membrane pairs, which is consistent with theoretical predictions. Likewise, system resistances measured for 1 to 5 IEM pairs were 3.07, 3.58, 4.09, 4.42, and 4.91 Ω, respectively. This progressive increase was attributed to the inherent resistance of IEMs, which selectively facilitate ion transport while contributing additional resistance to the system. The increase in resistance followed an approximately linear trend, reflecting the cumulative effect of each added membrane pair.

Fig. 7(b) shows the power density as a function of voltage for different numbers of IEM pairs. The corresponding power densities for 1 to 5 IEM pairs were 0.064, 0.183, 0.298, 0.306, and 0.328 W/m², respectively. Increasing the number of IEM pairs led to a higher OCV; however, it also increased the overall stack resistance due to the additional membrane pairs. Despite the increase in resistance, the net effect on power density remained favorable within the tested range. These results indicate that increasing the number of IEM pairs is a beneficial strategy for RED system design. Although additional membrane pairs contribute to increased resistance, the corresponding rise in system voltage enables greater power output.

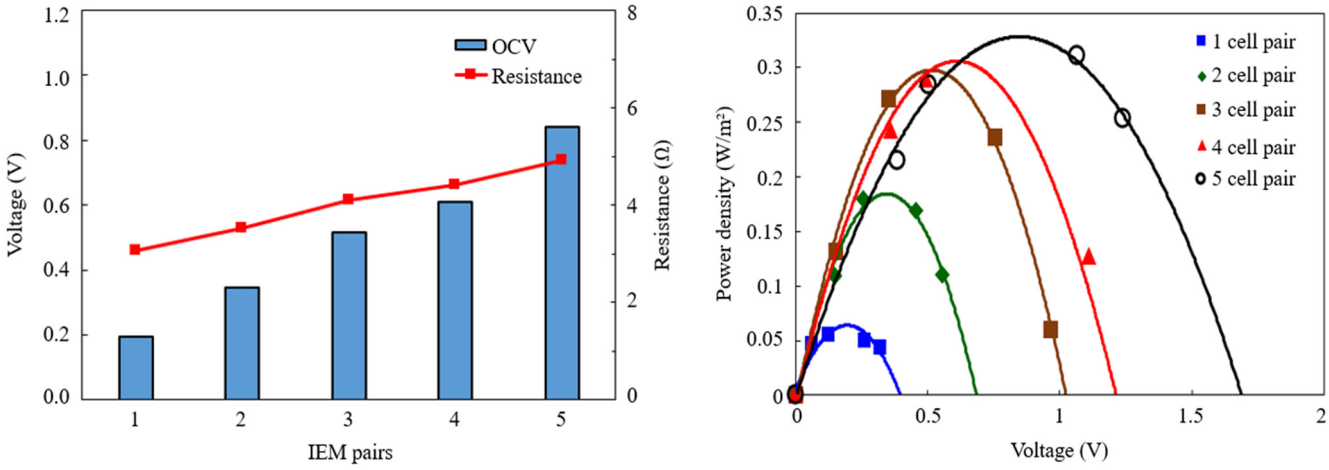

(a) OCV and internal resistance at different numbers of IEM pairs

(b) Power density versus voltageat different numbers of IEM pairs

Fig. 7 Effect of IEM pairs on RED system performance (HC: 1 M, LC: 0.02 M; space velocity: 0.25 1/min)

3.4. *Effects of flow channel thickness*

A series of experiments was conducted using flow channels with thicknesses of 1, 2, 3, and 4 mm, employing a single pair of IEMs under otherwise constant operating conditions (HC: 1 M, LC: 0.02 M, space velocity: 0.25 1/min). The relationship between OCV and internal resistance as a function of flow channel thickness in the RED stack is shown in Fig. 8(a). The OCV exhibited a modest increase with increasing flow channel thickness, likely due to the larger solution volume providing a higher concentration of mobile ions, which marginally enhances the membrane potential. The system resistances measured for channel thicknesses of 1, 2, 3, and 4 mm were 3.07, 4.36, 6.04, and 11.46 Ω, respectively, reflecting a consistent and substantial increase in resistance with increasing thickness. This trend is particularly pronounced at larger thicknesses and can be primarily attributed to the low conductivity of the LC solution.

Fig. 8(b) presents the power density as a function of voltage for different flow channel thicknesses. The corresponding power densities for channel thicknesses of 1, 2, 3, and 4 mm were 0.372, 0.416, 0.361, and 0.206 W/m², respectively. Among these, the 2 mm flow channel yielded the highest power density. The results indicate that increasing the flow channel thickness can lead to a slight enhancement in OCV, which is beneficial for power density. However, this advantage is counterbalanced by a corresponding increase in system resistance, which negatively affects overall power output. As a result, the power density initially exhibits a modest increase with flow channel thickness but subsequently declines. In particular, at a thickness of 4 mm, a sharp increase in resistance was observed, resulting in a substantial drop in power density.

While greater flow channel thickness may improve OCV by accommodating a larger number of ions, this benefit becomes marginal in system configurations involving a greater number of IEM pairs. In contrast, the impact of increased flow channel thickness on system resistance becomes more pronounced, posing a significant limitation to power density. Therefore, excessive channel thickness is ultimately detrimental to RED system performance and should be carefully optimized in system design.

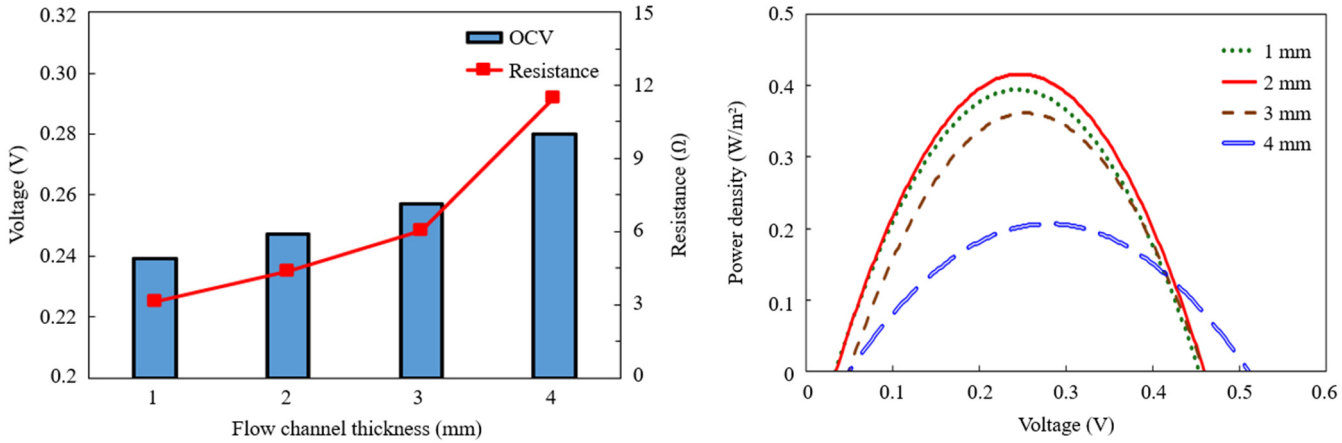

(a) OCV and internal resistance as a function of flow channel thickness

(b) Power density versus voltage for different flow channel thicknesses

Fig. 8 Effect of flow channel thickness on RED system performance (1 IEM pair; HC:1 M, LC: 0.02 M; space velocity: 0.25 1/min)

3.5. Benchmarking against prior RED studies

Table 1 Literature benchmark of representative RED operating conditions

Description (HC–LC, M)	S (cm²)	N	ERS type	V (1/min)	P_d (W/m²)	Ref.
0.02 / 2 M NaCl	67.5	5	0.02 M $Fe(CN)_6^{3-}$ / $Fe(CN)_6^{4-}$	0.25	0.446	This study
0.02 / 1 M NaCl	67.5	5	0.02 M $Fe(CN)_6^{3-}$ / $Fe(CN)_6^{4-}$	0.25	0.328	This study
RED operating on 0.006 / 0.6 M NaCl for oxidation of ammonia and power output	10 × 27	50	0.0002-0.2 M NaCl and NH_4Cl	0.098	0.06	[24]
RED operating on 0.1 / 5 M NaCl for power generation	44 × 44	500	0.3 M $Fe(CN)_6^{3-}$ / $Fe(CN)_6^{4-}$ and 2.5 M NaCl	1.4	3.2	[26]
RED operating on 0.017 / 0.507 M NaCl with CO_2 bubble for power output	96.04	5	0.05 M $Fe(CN)_6^{3-}$ / $Fe(CN)_6^{4-}$ and 0.25 M NaCl	5	0.29	[27]
RED operating on 0.006 / 0.6 M NaCl with a flow battery	8 × 8	20	0.3 M $Fe(CN)_6^{3-}$, 1 M KOH, and 0.6 M NaCl (An) 0.2 M 2,6 DHAQ, 1 M KOH, and 0.6 M NaCl (Cat)	0.625	0.07	[25]

Notes: S: membrane area; N: number of IEM pairs; ERS: electrode rinse solution; V: space velocity of saline solutions; P_d: power density; An: anode; Cat: cathode

This section provides a compact benchmark for contextual comparison with representative RED studies. Table 2 summarizes operating descriptors that materially influence reported power density, including membrane area, number of IEM pairs, electrode rinse solution chemistry, and space velocities. The purpose is to provide a transparent context for readers rather than to rank performance across studies. Reported power density reflects the coupled effects of driving force, internal resistance (often governed by LC conductivity and channel geometry), polarization (flow-dependent), and variations in electrode systems and operating definitions. Table 2 is therefore used to support design interpretation: balancing OCV gain against resistance penalties, selecting a practical flow regime that mitigates polarization without excessive hydraulic demand, and managing resistance accumulation when increasing IEM pairs, while acknowledging the limits of cross-study comparability.

4. Conclusions

This study systematically investigated the power generation performance of RED by evaluating the effects of key operating parameters, including the HC and LC solution concentrations, space velocity, number of IEM pairs, and flow channel thickness. The main conclusions are summarized as follows:

(1) A concentration ratio of HC to LC greater than 50:1 is required to provide sufficient Gibbs free energy for effective power generation in the RED system.

(2) The LC solution concentration should be maintained in the range of 0.02 to 0.05 M NaCl to balance ionic conductivity and internal resistance, while an HC solution concentration of 1 to 2.5 M NaCl provides an adequate salinity gradient without incurring high operational costs.

(3) An optimal space velocity of 0.25 1/min for both HC and LC streams enables efficient ion transport while minimizing pumping energy consumption.

(4) Increasing the number of IEM pairs significantly improves OCV and power density; however, the associated increase in internal resistance must be carefully managed to maintain system efficiency.

(5) A flow channel thickness of 1 to 2 mm effectively enhances ion exchange while limiting resistance losses, thereby improving the overall RED performance.

Overall, this study provides comprehensive guidance for optimizing RED system operation and contributes to the advancement of salinity gradient energy as a viable renewable energy technology. Further investigations should focus on scaling up the RED system by increasing the number of membrane pairs and the active membrane area to evaluate performance under conditions closer to practical applications. In addition, the use of real feed waters, such as seawater, river water, and desalination brine, should be examined to assess the effects of multivalent ions, organic matter, and fouling on long-term system stability.

Abbreviations

SGP	Salinity gradient power		SD	Swelling degree
RED	Reverse electrodialysis		IEC	Ion-exchange capacity
HC	High-concentration		FCD	Fixed charge density
LC	Low-concentration		CEM	Cation-exchange membrane
IEM	Ion-exchange membrane		AEM	Anion-exchange membrane
OCV	Open circuit voltage		DSA	Dimensionally stable anode

Conflicts of Interest

The authors declare no conflict of interest.

References

[1] J. N. Weinstein and F. B. Leitz, "Electric Power from Differences in Salinity: The Dialytic Battery," Science, vol. 191, no. 4227, pp. 557-559, 1976.

[2] C. Simões, B. Vital, T. Sleutels, M. Saakes, and W. Brilman, "Scaled-Up Multistage Reverse Electrodialysis Pilot Study with Natural Waters," Chemical Engineering Journal, vol. 450, part 4, article no. 138412, 2022.

[3] J. Veerman, "Concepts and Misconceptions concerning the Influence of Divalent Ions on the Performance of Reverse Electrodialysis Using Natural Waters," Membranes, vol. 13, no. 1, article no. 69, 2023.

[4] A. Emdadi, L. F. Greenlee, and B. Logan, "Uphill Transport of Sulfate and Chloride Ions under Different Operational Conditions of a Reverse Electrodialysis (RED) Stack," Chemical Engineering Journal, vol. 508, article no. 160897, 2025.

[5] L. N. Nthunya, M. F. Bopape, O. T. Mahlangu, B. B. Mamba, B. Van der Bruggen, C. A. Quist-Jensen, et al., "Fouling, Performance and Cost Analysis of Membrane-Based Water Desalination Technologies: A Critical Review," Journal of Environmental Management, vol. 301, article no. 113922, 2022.

[6] S. K. Al Dawery, M. K. Al-Sawai, G. M. S. Al Muzami, S. H. K. Annamareddy, M. S. Al Dawari, R. H. Harharah, et al., "Treatment of Produced Water Using Prepared Activated Carbon-Based Sewage Sludge," Separations, vol. 10, no. 10, article no. 519, 2023.

[7] V. M. Ortiz-Martínez, L. Gómez-Coma, C. Tristán, G. Pérez, M. Fallanza, A. Ortiz, et al., "A Comprehensive Study on the Effects of Operation Variables on Reverse Electrodialysis Performance," Desalination, vol. 482, article no. 114389, 2020.

[8] J. Li, C. Zhang, Z. Wang, H. Wang, Z. Bai, and X. Kong, "Power Harvesting from Concentrated Seawater and Seawater by Reverse Electrodialysis," Journal of Power Sources, vol. 530, article no. 231314, 2022.

[9] T. Xu, "Ion Exchange Membranes: State of Their Development and Perspective," Journal of Membrane Science, vol. 263, no. 1-2, pp. 1-29, 2005.

[10] T. Sata, Ion Exchange Membranes: Preparation, Characterization, Modification and Application, 2nd ed., London: Royal Society of Chemistry, 2007.

[11] D. A. Vermaas, M. Saakes, and K. Nijmeijer, "Doubled Power Density from Salinity Gradients at Reduced Intermembrane Distance," Environmental Science & Technology, vol. 45, no. 16, pp. 7089-7095, 2011.

[12] F. Helfer, C. Lemckert, and Y. G. Anissimov, "Osmotic Power with Pressure Retarded Osmosis: Theory, Performance and Trends – A Review," Journal of Membrane Science, vol. 453, pp. 337-358, 2014.

[13] E. Güler, R. Elizen, D. A. Vermaas, M. Saakes, and K. Nijmeijer, "Performance-Determining Membrane Properties in Reverse Electrodialysis," Journal of Membrane Science, vol. 446, pp. 266-276, 2013.

[14] E. Guler, Y. Zhang, M. Saakes, and K. Nijmeijer, "Tailor-Made Anion-Exchange Membranes for Salinity Gradient Power Generation Using Reverse Electrodialysis," ChemSusChem, vol. 5, no. 11, pp. 2262-2270, 2012.

[15] A. Ranade, K. Singh, A. Tamburini, G. Micale, and D. A. Vermaas, "Feasibility of Producing Electricity, Hydrogen, and Chlorine via Reverse Electrodialysis," Environmental Science & Technology, vol. 56, no. 22, pp. 16062-16072, 2022.

[16] T. F. Gül, M. Akalın, E. N. Dönmezler, A. Bolat, A. Cihanoğlu, E. Güler, et al., "Review on Reverse Electrodialysis Process-A Pioneering Technology for Energy Generation by Salinity Gradient," Frontiers in Membrane Science and Technology, vol. 3, article no. 1414721, 2024.

[17] Y. Mei and C. Y. Tang, "Co-Locating Reverse Electrodialysis with Reverse Osmosis Desalination: Synergies and Implications," Journal of Membrane Science, vol. 539, pp. 305-312, 2017.

[18] M. Sharma, P. P. Das, A. Chakraborty, and M. K. Purkait, "Clean Energy from Salinity Gradients Using Pressure Retarded Osmosis and Reverse Electrodialysis: A Review," Sustainable Energy Technologies and Assessments, vol. 49, article no. 101687, 2022.

[19] N. Y. Yip and M. Elimelech, "Thermodynamic and Energy Efficiency Analysis of Power Generation from Natural Salinity Gradients by Pressure Retarded Osmosis," Environmental Science & Technology, vol. 46, no. 9, pp. 5230-5239, 2012.

[20] D. A. Vermaas, J. Veerman, N. Y. Yip, M. Elimelech, M. Saakes, and K. Nijmeijer, "High Efficiency in Energy Generation from Salinity Gradients with Reverse Electrodialysis," ACS Sustainable Chemistry & Engineering, vol. 1, no. 10, pp. 1295-1302, 2013.

[21] J. W. Post, H. V. M. Hamelers, and C. J. N. Buisman, "Energy Recovery from Controlled Mixing Salt and Fresh Water with a Reverse Electrodialysis System," Environmental Science & Technology, vol. 42, no. 15, pp. 5785-5790, 2008.

[22] J. Veerman, J. W. Post, M. Saakes, S. J. Metz, and G. J. Harmsen, "Reducing Power Losses Caused by Ionic Shortcut Currents in Reverse Electrodialysis Stacks by a Validated Model," Journal of Membrane Science, vol. 310, no. 1-2, pp. 418-430, 2008.

[23] M. Tedesco, C. Scalici, D. Vaccari, A. Cipollina, A. Tamburini, and G. Micale, "Performance of the First Reverse Electrodialysis Pilot Plant for Power Production from Saline Waters and Concentrated Brines," Journal of Membrane Science, vol. 500, pp. 33-45, 2016.

[24] Y. Zhou, K. Zhao, C. Hu, H. Liu, Y. Wang, and J. Qu, "Electrochemical Oxidation of Ammonia Accompanied with Electricity Generation Based on Reverse Electrodialysis," Electrochimica Acta, vol. 269, pp. 128-135, 2018.

[25] X. Zhu, T. Kim, M. Rahimi, C. A. Gorski, and B. E. Logan, "Integrating Reverse-Electrodialysis Stacks with Flow Batteries for Improved Energy Recovery from Salinity Gradients and Energy Storage," ChemSusChem, vol. 10, no. 4, pp. 797-803, 2017.

[26] M. Tedesco, A. Cipollina, A. Tamburini, and G. Micale, "Towards 1 kw Power Production in a Reverse Electrodialysis Pilot Plant with Saline Waters and Concentrated Brines," Journal of Membrane Science, vol. 522, pp. 226-236, 2017.

[27] J. Moreno, N. de Hart, M. Saakes, and K. Nijmeijer, "CO2 Saturated Water As Two-Phase Flow for Fouling Control in Reverse Electrodialysis," Water Research, vol. 125, pp. 23-31, 2017.